ISSN1027-5495. Functional Materials, 32, No.3 (2025), p. 372-379
doi:http://dx.doi.org/10.15407/fm32.03.372 © 2025 — STC "Institute for Single Crystals"

Synthesis, electronic structure and morphological features of composite films based on ZnO and calcium hydroxyapatite for conductive layers of solar cells with encapsulating properties

N.A. Kurgan[1], V.L. Karbivskyi[1], S.I. Shulyma[1], N.K. Shvachko[1], V.V. Zaika[1], V.O. Moskaliuk[1], L.P. Kliuienko, S.P. Starik[2]

[1]Kurdyumov Institute of Metallophysics of the National Academy of Sciences of Ukraine, 36 Vernadsky Blvd. 03142, Kyiv, Ukraine
[2]Bakul Institute of Superhard Materials of the National Academy of Sciences of Ukraine, 2 Avtozavodska St., 04074, Kyiv, Ukraine

Received February 22, 2025

For the first time, the structural and morphological characteristics of ZnO-apatite composite films at varying concentrations of apatite have been comprehensively studied for practical applications as a current-carrying layer of solar cells with encapsulating properties. Notably, surface nanoclusters with a characteristic size of approximately 10 nm have been observed. Furthermore, the peculiarities of electron charge redistribution during the formation of the ZnO/apatite interface have been elucidated. This process involves a redistribution of electron density on the oxygen atoms and an enhancement of symmetry around the PO_4 tetrahedra. Additionally, it has been determined that an increase in the calcium hydroxoapatite content in the film leads to a widening of the band gap in comparison to pure ZnO. The most optimal characteristics are achieved for the encapsulating layer of ZnO/apatite with a component ratio of 3:1.

Keywords: calcium hydroxyapatite, thin films, ZnO, magnetron sputtering, electronic structure, morphological features, solar cells.

Створення, електронна будова та морфологічні особливості композитних плівок на основі ZnO та гідроксоапатиту кальцію для струмозйомних шарів сонячних елементів з капсулюючими властивостями. *Н.А. Курган, В.Л. Карбівський, С.І. Шулима, Н.К. Швачко, В.В. Заїка, В.О. Москалюк, Л.П.Клюєнко, С.П. Старик*

Вперше отримано та всебічно досліджено структурні та морфологічні особливості композитних плівок ZnO-апатит за різної концентрації апатиту з метою практичного застосування в якості струмозйомного шару сонячних комірок з капсулюючими властивостями. Спостерігається утворення поверхневих нанокластерів з характерним розміром ~ 10 нм. Встановлено особливості перерозподілу електронного заряду при формуванні інтерфейсу ZnO/апатит. Відбувається перерозподіл електронної густини на атомах кисню та підвищення симетрії навколо PO_4 тетраедрів. Визначено, що при збільшенні вмісту гідроксоапатиту кальцію у плівці, спостерігається збільшення ширини забороненої зони, порівняно з чистим ZnO. Найбільш оптимальні характеристики має капсулюючий шар ZnO/апатит зі співвідношенням компонентів 3:1.

1. Introduction

The design of highly efficient solar cells is currently a critical area of green energy development. However, the widespread adoption of solar panels is hindered by three primary factors: the high cost of solar cells, their dependence on weather conditions, and complex production technology. In recent years, a novel technology of solar modules based on perovskites has made significant progress in this field [1-5]. The unique properties of the perovskite crystal lattice make it possible to manufacture an exceptionally efficient light-collecting layer for solar cells. These solar cells exhibit a prolonged service life, a broad spectrum of light absorption, and a high absorption coefficient of incident radiation [4]. The most prevalent compound in perovskite photovoltaics is lead-methylammonium iodide ($CH_3NH_3PbX_3$), where X typically denotes iodine or bromine/chloride [6]. The main obstacle to the widespread adoption of perovskite solar panels is their dependence on external influences. Humidity, elevated temperatures, and sunlight all influence the efficiency of the perovskite layer within solar cells, leading to its decomposition. Additionally, lead pollution poses a potential threat to both animals and the environment [7]. This problem can be solved by encapsulating a layer of perovskite inside the cell. However, such encapsulation does not address the challenges of long-term stability and the release of toxic lead from used or damaged solar cells [8-9]. In this regard, intensive search materials for the protective active layer of cells and the creation of a more durable interface have been undertaken. Recent studies in this domain have demonstrated the effectiveness of utilizing calcium hydroxyapatite to trap toxic ions in damaged perovskite elements [10 -15]. Calcium hydroxyapatite (HAp, $Ca_{10}(PO_4)_6(OH)_2$) is a biocompatible material that is widely used in various industries and is absolutely safe for the environment [16-18]. The crystal structure of HAp remains practically unchanged in a wide range of deviations from the stoichiometric composition (Ca:P=1.66), and OH^- ions are stable even at high temperatures (up to 1350 °C), which allows the use of such materials as sorbents for heavy metals and matrices for the disposal of radioactive waste [19-23]. In this regard, it has potential as a promising encapsulating layer for solar cells [24].

This paper presents the results of the design of a conductive electron transport layer using calcium hydroxyapatite and zinc oxide in the form of thin films. The most commonly used material for such a transport layer is titanium dioxide. However, recent studies have shown greater efficiency in using ZnO instead of titanium oxide, which has similar energy characteristics but higher electron mobility [25]. An additional advantage of ZnO is that its synthesis and processing do not require high temperatures [26].

2. Experimental

Target for ZnO and calcium hydroxyapatite composite films ($Ca_{10}(PO_4)_6((OH)_2$) was prepared from a mixture of powders ZnO: $Ca_{10}(PO_4)_6((OH)_2$ in weight ratios 75:25 and 50:50. The average particle size of the original calcium hydroxyapatite powder was 49.5±1.7 nm. The initial ZnO powder was a globule of several microns. The films were obtained by radiofrequency magnetron sputtering (13.56 ± 0.135 MHz). The powders were mixed in the proper weight ratio, stirred thoroughly for an hour, and pressed into the mold using a hydraulic press under a load of 10 ton/ cm^2. Immediately after the target was pressed, it was transported to the chamber of the vacuum universal post (VUP-5M), where composite films were synthesized. The sputtering process was carried for an hour. The films were deposited on 1x1 cm^2 microscopic glass slides, which were pre-washed in an ultrasonic bath in acetone, isopropyl alcohol for 30 minutes, then rinsed with deionized water, and the remaining water was blown off with dry nitrogen N_2 (99,9%). The distance from the target to the substrate was 4.5 cm, and the pressure during the synthesis in the vacuum chamber was 1×10^{-2} Pa. Argon (99.9%) at a pressure of 1.3 Pa was used to generate plasma. The films were deposited at a magnetron power of 80 W. Five samples of films of each composition were obtained.

X-ray diffraction patterns were obtained using a MiniFlex 600 diffractometer (Rigaku, Japan) (radiation Cu-$K\alpha$, λ = 1.5418740 Å). The measurements were carried out using a θ-2θ scanning scheme with Bragg-Brentano focusing in the 2θ angle range from 5 to 90° with a step of $\Delta(2\theta)$ = 0.02°. The exposure time at each point was 1 second. Electron microscopy images of the samples were obtained using a TESCAN MIRA3 scanning electron microscope (SEM) with an accelerating voltage of 5 – 20 kV. Energy dispersive analysis was carried out using an in-line Oxford X-max 80 mm^2 unit.

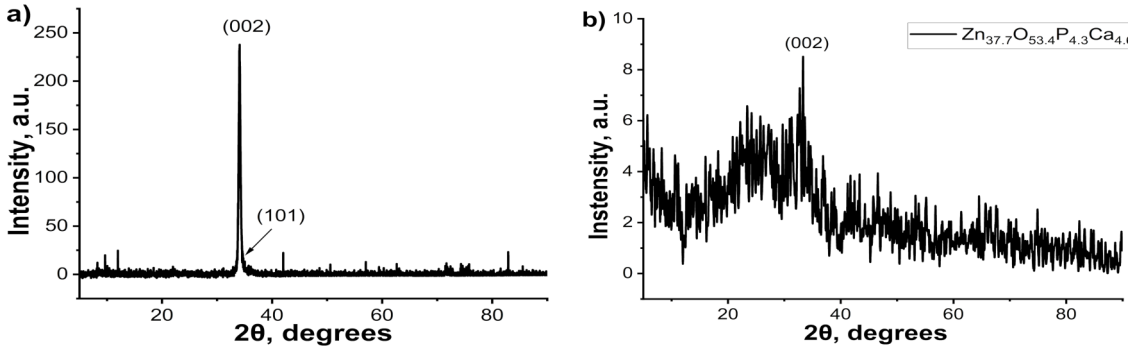

Fig. 1. Diffraction patterns of: a) ZnO film, b) composite film $Zn_{37.7}O_{53.4}P_{4.3}Ca_{4.6}$.

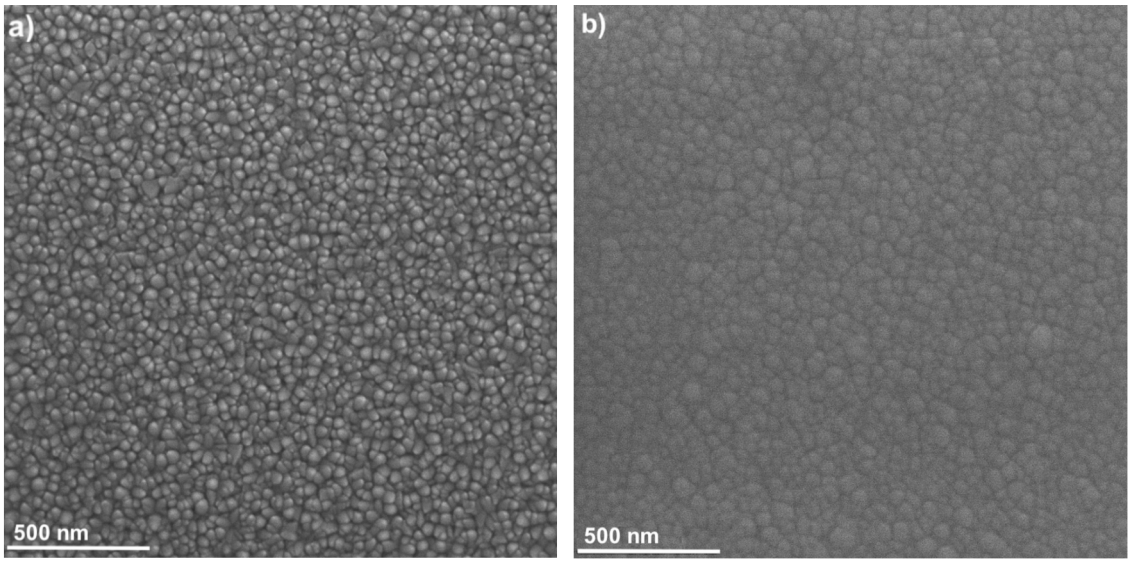

Fig. 2. SEM images of the film surface: a) ZnO, and b) $Zn_{37.7}O_{53.4}P_{4.3}Ca_{4.6}$.

The optical absorption spectra of the samples were obtained using a Spekol 1500 spectrophotometer in the wavelength range of 190-1100 nm. The width of the optical band gap (E_g) was estimated using the Tauc equation [27], in which the energy-dependent adsorption coefficient (α) is calculated using the expression: $(\alpha h\nu)^{1/\gamma} = B(h\nu - E_g)$, where h is Planck's constant, ν is the frequency and B is the constant. The parameter γ is related to the type of electron transition. For a direct permitted transition, $\gamma = ½$, and for an indirect permitted transition, $\gamma = 2$ [28]. Since the films were formed from a mixture of powders of ZnO, which is a direct-bandgap semiconductor, and GAP, which has an indirect transition [23], the transition was considered indirect for the formed complex of compounds.

The X-ray photoelectron spectra (XPS) of the core-state levels of the studied elements were obtained using an XPS 2400 X-ray spectrometer (Jeol, Japan). The working vacuum during the experiment was 10^{-7} Pa. A magnesium anode with energy of 1253.6 eV of the Mg K_α line was used. The energy resolution was 0.1 eV. The binding energies were calibrated using the 1*s* line of carbon at 284.0 eV. The nanorelief of the surface of the samples was studied by scanning tunneling microscopy (STM) using a JSPM-4610 device (Jeol, Japan). The vacuum in the tunneling microscope chamber was not lower than 10^{-7} Pa. The studies were carried out at room temperature.

3. Results and discussion

The elemental chemical composition of composite films obtained from a target of mixed ZnO (75%)/HAp (25%) and ZnO (50%)/HAp (50%) powders was determined by X-ray energy dispersive analysis. For films obtained from the ZnO:hydroxyapatite target in a weight ratio of 75:25, the elemental composition was $Zn_{37.7}O_{53.4}P_{4.3}Ca_{4.6}$ (Table 1). The elemental composition of the films obtained from the

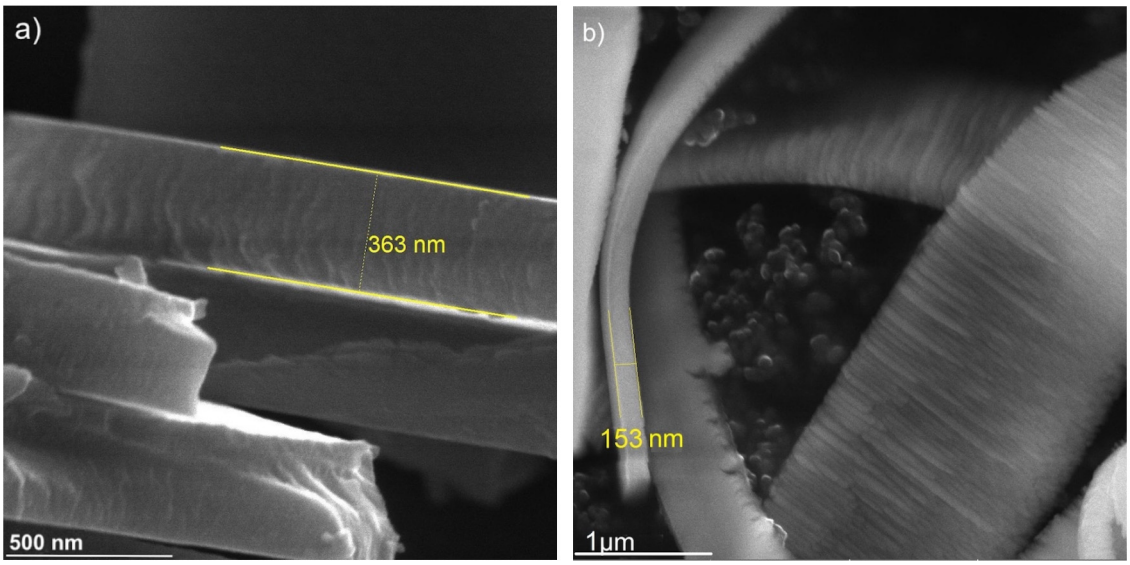

Fig. 3. SEM images of the film surface: a) $Zn_{37.7}O_{53.4}P_{4.3}Ca_{4.6}$ and b) $Zn_{25.2}O_{56.9}P_{8.3}Ca_{9.6}$.

ZnO:hydroxyapatite target in a weight ratio of 50:50 was $Zn_{25.2}O_{56.9}P_{8.3}Ca_{9.6}$. The number of zinc atoms correlates with their number in the initial mixture of powders. For the stoichiometric HAp, the ratio between Ca/P atoms is 1.66, but in our case, these values were 1.07 for the $Zn_{37.7}O_{53.4}P_{4.3}Ca_{4.6}$ sample, and 1.16 for the $Zn_{25.2}O_{56.9}P_{8.3}Ca_{9.6}$ sample.

The results of the X-ray diffraction study of the structure of the $Zn_{37.7}O_{53.4}P_{4.3}Ca_{4.6}$ composite film showed (Fig. 1) that, in contrast to the pure ZnO film (Fig. 1a), no narrow and clear diffraction peaks are observed for the composite film (Fig. 1b). The observed diffraction pattern is characterized by broad, low-intensity halo peaks, typical of amorphous materials. However, unlike fully amorphous samples, a low-intensity diffraction peak at 33.3° is observed, indicating that the film is somewhat textured.

The surfaces of both films show signs of nanostructure with grains of varying shapes, which are generally round (Fig. 2). The average grain size for the $Zn_{37.7}O_{53.4}P_{4.3}Ca_{4.6}$ samples was 41.8 nm, with a standard deviation of 13.8 nm, which is slightly larger than the average grain size of ZnO films of 34.0±8.3 nm. The films are also characterized by significant dispersion, since the smallest grain size was 21.9 nm and the largest was 76.4 nm. For the $Zn_{25.2}O_{56.9}P_{8.3}Ca_{9.6}$ sample, SEM image of the surface could not be obtained due to its poor conductivity.

To estimate the thickness of the films, they were destroyed, and their cross-sectional images were obtained by SEM (Fig. 3). It can be seen from this figure that the film thickness was ~363 nm for $Zn_{37.7}O_{53.4}P_{4.3}Ca_{4.6}$ (Fig. 3a), and ~153 nm for $Zn_{25.2}O_{56.9}P_{8.3}Ca_{9.6}$ (Fig. 3b). The cross-sectional images also show a slight texture that correlates with the X-ray diffraction data.

Since the texture of the films affects the sorption properties of the surface, STM images of the surface of the $Zn_{37.7}O_{53.4}P_{4.3}Ca_{4.6}$ sample were studied in detail (Fig. 4). Due to the poor conductivity of the $Zn_{25.2}O_{56.9}P_{8.3}Ca_{9.6}$ sample, a STM image of the film surface was not obtained.

It can be seen that the surface of the $Zn_{37.7}O_{53.4}P_{4.3}Ca_{4.6}$ film consists of small formations up to 10 nm in size (Fig. 4). The roughness parameters were estimated as follows: R_a = 0.59 nm, R_q = 0.74 nm, R_{zjis} = 4.82 nm, R_z = 5.70 nm for image 4(a). For image 4(b), the roughness parameters were: R_a = 1.03 nm, R_q = 1.20 nm, R_{zjis} = 7.01 nm, R_z = 7.61 nm,

Table 1: Quantitative chemical analysis of thin films by X-ray energy dispersive spectroscopy

Sample	O (at. %)	P (at. %)	Ca (at. %)	Zn (at. %)
$Zn_{37.7}O_{53.4}P_{4.3}Ca_{4.6}$	53.4	4.3	4.6	37.7
$Zn_{25.2}O_{56.9}P_{8.3}Ca_{9.6}$	56.9	8.3	9.6	25.2

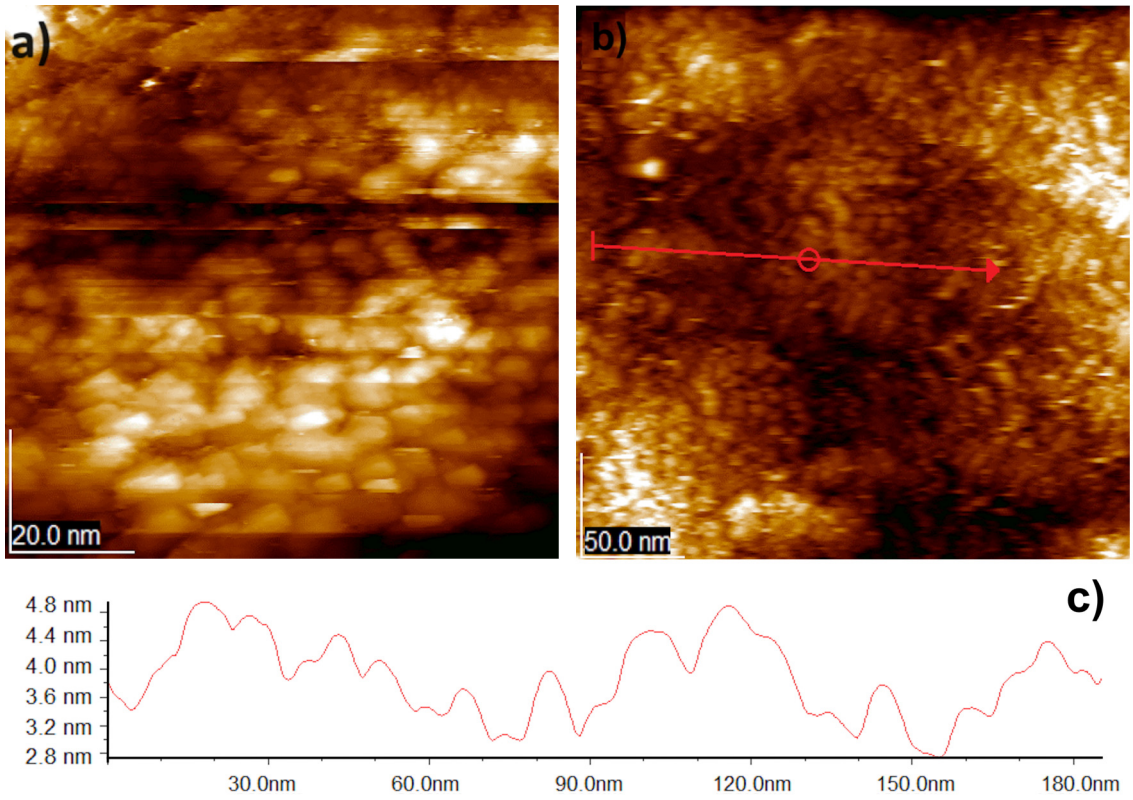

Fig. 4. a, b) STM images of the surface of the $Zn_{37.7}O_{53.4}P_{4.3}Ca_{4.6}$ film; c) surface profile along the line shown in Fig. 4(b).

which indicates a sufficiently smooth surface over a sufficiently large area under study. Due to the small roughness parameters, it is difficult to separate the individual grains in the SEM images. However, based on the surface profile, their height can be estimated to be approximately 2 nm (Fig. 4c).

To clarify the changes in the electronic subsystem during the formation of the ZnO/HAp interface, we obtained the XPS spectra of atomic levels of elements of the studied composite films and compared them with the data for pure HAp and ZnO (Fig. 5). The Zn $2p_{3/2}$ binding energy for all composite films has a maximum of 1021.3 eV, and coincides with the value for ZnO films within the experimental error [29]. The full width at half maximum (FWHM) value of the Zn $2p_{3/2}$ peaks increases from 1.96 eV [29] for ZnO to 2.18 eV for $Zn_{25.2}O_{56.9}P_{8.3}Ca_{9.6}$ films, indicating a change in the chemical environment of zinc atoms during the formation of the ZnO/HAp interface, including due to an increase in the number of defects.

For the O 1*s* spectrum (Fig. 5 b), a shift of the main maximum towards higher binding energies is observed for the sample $Zn_{37.7}O_{53.4}P_{4.3}Ca_{4.6}$, which indicates a lower electron density on oxygen atoms compared to the sample $Zn_{25.2}O_{56.9}P_{8.3}Ca_{9.6}$. That is, during the formation of the ZnO/HAp interface, the electron density on oxygen atoms is redistributed.

Based on the values of the binding energy for P *2p* for HAp and the $Zn_{37.7}O_{53.4}P_{4.3}Ca_{4.6}$ composite film, it can be argued that PO_4 tetrahedra are preserved during magnetron sputtering (Fig. 5c). However, a decrease in the FWHM parameter for both composite films can be explained by an increase in symmetry around the PO_4 tetrahedra. For the $Zn_{25.2}O_{56.9}P_{8.3}Ca_{9.6}$ sample, a shift towards higher binding energies for the P *2p* levels is observed (Table 2) compared to the HAp.

Thus, summarizing the results of the XPS analysis, it can be noted that the formation of the ZnO/HAp interface preserves the chemical bonds zinc-oxygen and phosphorus-oxygen with some distortions of the PO_4 tetrahedral sublattice of calcium hydroxyapatite.

In order to determine the optical characteristics and clarify the conductive properties, the obtained films were studied by spectrophotometry with the calculation of the band gap using the Tauc method. The optical trans-

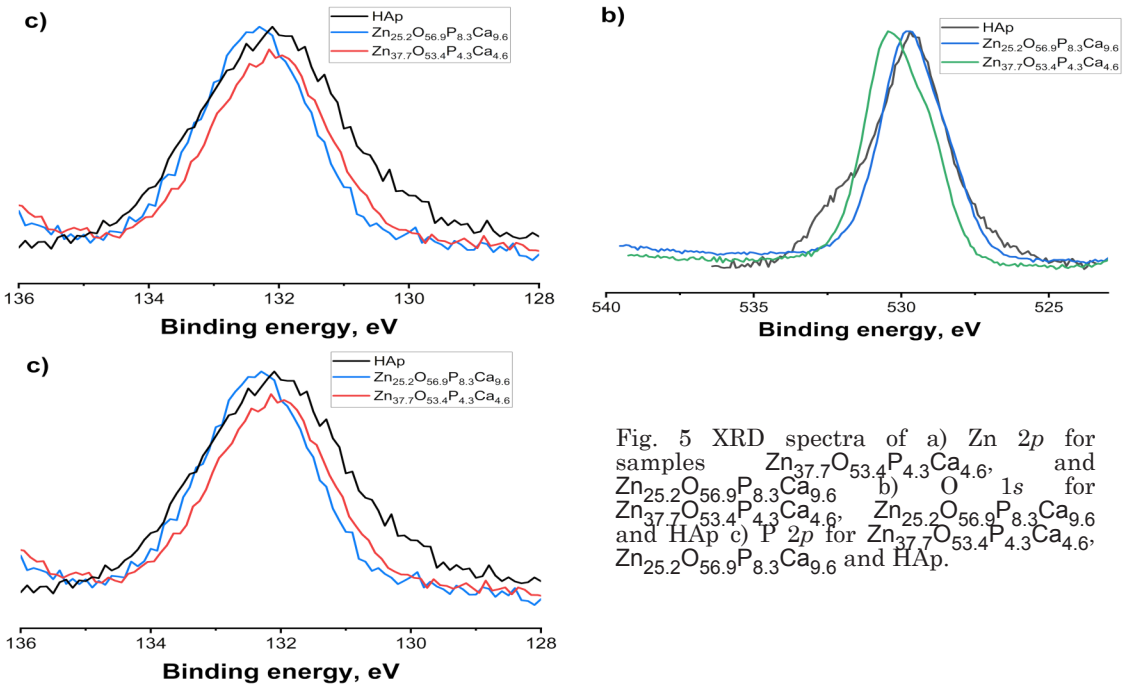

Fig. 5 XRD spectra of a) Zn 2*p* for samples $Zn_{37.7}O_{53.4}P_{4.3}Ca_{4.6}$, and $Zn_{25.2}O_{56.9}P_{8.3}Ca_{9.6}$ b) O 1*s* for $Zn_{37.7}O_{53.4}P_{4.3}Ca_{4.6}$, $Zn_{25.2}O_{56.9}P_{8.3}Ca_{9.6}$ and HAp c) P 2*p* for $Zn_{37.7}O_{53.4}P_{4.3}Ca_{4.6}$, $Zn_{25.2}O_{56.9}P_{8.3}Ca_{9.6}$ and HAp.

mittance spectra of the ZnO/HAp composite films are shown in Fig. 6. It can be seen that the composite films $Zn_{37.7}O_{53.4}P_{4.3}Ca_{4.6}$ and $Zn_{25.2}O_{56.9}P_{8.3}Ca_{9.6}$ are characterized by high transparency in the entire visible spectral range (Fig. 6a). The highest transparency value in the visible spectral range was observed for the $Zn_{37.7}O_{53.4}P_{4.3}Ca_{4.6}$ film: the transmittance was 92.5±0.5 % at a wavelength of 500±2 nm; and the $Zn_{25.2}O_{56.9}P_{8.3}Ca_{9.6}$ sample had a transmittance of 92.0±0.5 % at a wavelength of 777±2 nm. The observed oscillations for the $Zn_{37.7}O_{53.4}P_{4.3}Ca_{4.6}$ sample are associated with interference effects and confirm the smooth surface of the film. For a more detailed study of the optical properties of the $Zn_{37.7}O_{53.4}P_{4.3}Ca_{4.6}$ film, additional studies were performed for films obtained at a sputtering time of 15 min (film thickness ~ 100 nm) and the results were compared with the available data (Fig. 6b). The absorption peak was shifted toward shorter wavelengths compared to the film deposited for 60 min. For a film of this thickness, oscillatory effects were absent.

The calculated value of the band gap of the $Zn_{25.2}O_{56.9}P_{8.3}Ca_{9.6}$ sample was E_g ~ 4.2 eV, which confirms its dielectric behavior and is the average value between the band gaps of the individual components of the composite film. In this case, the average value between 3.2 eV (ZnO) and 5.2 eV (calcium hydroxyapatite) is approximately 4.2 eV.

The width of the optical bandgap for the $Zn_{37.7}O_{53.4}P_{4.3}Ca_{4.6}$ sample showed two values of 3.2 eV and 3.8 eV (Fig. 7), which confirms the conductivity of the obtained film. The first value corresponds to the E_g value for pure ZnO. However, the second value is not the average value between the band gaps of the individual components of the composite film and indicates the interaction between ZnO and calcium hydroxyapatite during the forming of the interface and the emergence of new energy states that reduce the width of the band gap. This may be the result of the formation of a new phase with such a band gap.

Table 2. Binding energy P *2p* and the FWHM parameter

Sample	Binding energy P *2p*, eV	FHWM, eV
HAp	132.1	2.71
$Zn_{25.2}O_{56.9}P_{8.3}Ca_{9.6}$	132.3	1.95
$Zn_{37.7}O_{53.4}P_{4.3}Ca_{4.6}$	132.1	2.08

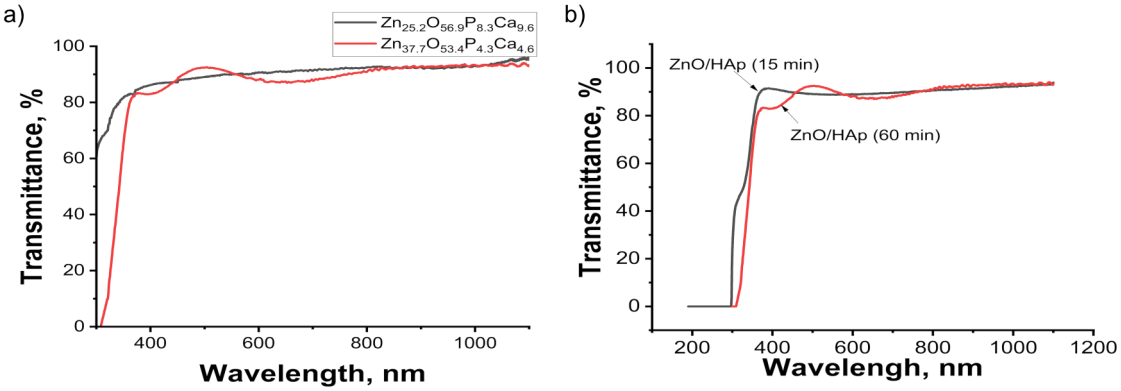

Fig. 6. Transmittance spectra of: a) $Zn_{37.7}O_{53.4}P_{4.3}Ca_{4.6}$ and $Zn_{25.2}O_{56.9}P_{8.3}Ca_{9.6}$ composite films; b) $Zn_{37.7}O_{53.4}P_{4.3}Ca_{4.6}$ films obtained at different sputtering times (15 and 60 minutes).

4. Conclusions

For the first time, ZnO-HAp composite films with a concentration of calcium hydroxoapatite of 25 wt.% and 50 wt.% were obtained by the method of magnetron sputtering. Their practical application as a conductive layer was investigated.

It has been demonstrated that the formation of films results in the creation of amorphous nanostructures characterized by minimal texture. Surface nanoclusters with a characteristic size of ~10 nm are observed.

During the formation of the ZnO/HAp interface, the preservation of zinc-oxygen and phosphorus-oxygen chemical bonds with some distortions of the PO_4 tetrahedral sublattice of calcium hydroxoapatite is observed.

Composite films based on ZnO with HAp in a ratio of 3:1 (25 wt.% HAp) retain electrical conductivity in contrast to films with a HAp content of 50 wt.%. With an increase in the content of HAp in the film, the width of the band gap increases compared to pure ZnO.

The results of our research indicate the possibility of practical application of ZnO-HAp composite film (75/25 wt.%) as a conductive layer of solar cells with encapsulating properties.

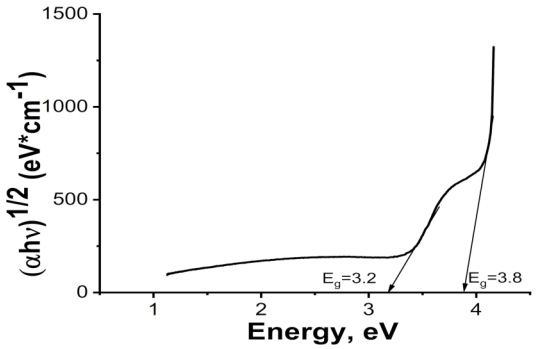

Fig. 7. Estimation of the band gap (E_g) of the sample $Zn_{37.7}O_{53.4}P_{4.3}Ca_{4.6}$ by the Tauc method.

References

1. I. Bąk, K. Cheba, *Green Energy. Green Energy and Technology. Springer, Cham,* 1-16 (2023).
2. O.A. Al-Shahri, F.B. Ismail, M.A. Hannan, *Journal of Cleaner Production* **284(19-E)**, 125465 (2021).
3. J. Yan, T. J. Savenije, L. Mazzarella and O. Isabella, *Sustainable Energy Fuels,* **6**, 243-266 (2022).
4. P. Roy, A. Ghosh, F. Barclay, et al., *Coatings,* **12(8)**, 1089 (2022).
5. Y. Zhao, Q. Ye, Z. Chu, et al., *Energy Environ. Mater., **2,*** 93-106 (2019).
6. N. Jeon, J. Noh, W. Yang, et al., *Nature,* **517**, *476–480* (2015).
7. P. Su, Y. Liu, J. Zhang, et al., *J. Phys. Chem. Lett.*, **11(8)**, 2812–2817 (2020).
8. H. Luo, P. Li, J Ma, et al., *Advanced Energy Materials*, **12(30),** 2201242 (2022).
9. R. K. Raman, S. a. G. Thangavelu, S. Venkataraj, A. Krishnamoorthy, *Renewable and Sustainable Energy Reviews*, **151(80)**, 111608 (2021).
10. S. Chen, Y. Deng, H. Gu, et al., *Nature Energy,* **5(12)**, 1003–1011 (2020).
11. X. Li, F. Zhang, H. He, et al., *Nature,* **578**, 555–558 (2020).
12. Y. Jiang, L. Qiu, E. J. Juarez-Perez, et al., *Nature Energy*, **4(9)**, 585–593 (2019).
13. M. Z. Mokhtar, A. Altujjar, B. Wang, et al., *Commun Mater*, **3(1)**, 77 (2022).
14. M.Z. Mokhtar, J. He, M. Li, et al., *Chem. Commun.*, **57(8)**, 994-997 (2021).
15. S. Y. Park, J.-S. Park, B. J. Kim, et al., *Nat. Sustain.* **3(12)**, 1044–1051 (2020).
16. D. Arcos, M. Vallet-Regí, *J. Mater. Chem.* **B 8(9)**, 1781–1800 (2020).
17. Y. Liu, Y. Tang, J. Wu, et al., *J. Colloid Interface Sci.* **570**, 402–410 (2020).

18. A. Das, D. Pamu, D.S. Gomes, et al., *Ceramica*, **65(374)**, 282–302 (2019).
19. A. P. Shpak, V. L. Karbovskii, N. A. Kurgan, et al., *Functional materials*, **12(4)**, 695—699 (2005)
20. V.L. Karbivskyy, A.P Shpak, N.A. Kurgan, et al., *J. Functional Materials*, **18(2)**, 195-199 (2011).
21. V. L. Karbivskyy, N. A. Kurgan, A.S. Litovchenko, et al., J. *Materials Science and Engineering*, **3(12)**, 52-56.
22. I. L. Balasooriya, J. Chen, S. M. K. Gedara, et al., Nanomaterials, **12(14)**, 2324 (2022).
23. Z. Li, Y. Qiu, D. Zhao, et al., *Sci Total Environ.* **904**, 166918 (2023).
24. V. Karbivskyy, N. Kurgan, M. Huntush, et al., *J. Appl. Phys.* **135(6)**, 065102 (2024).
25. A. Perez-Tomas, A. Mingorance, D. Tanenbaum, M. Lira-Cantu, *Elsevier*, **8**, 267-356 (2018).
26. C. Otalora, M. A. Botero, G. Ordoñez, *Journal of Materials Science*, **56(28**), 15538–15571 (2021).
27. J. Tauc, R. Grigorovici, A. Vancu, *Phys. Status Solidi*. (b) **15(2)**, 627–637 (1966).
28. P. Makuła, M. Pacia, W. Macyk, *J. Phys. Chem. Lett*. **9(23)**, 6814–6817 (2018).
29. V.V. Zaika, N.K. Shvachko, V.L. Karbivskyy, et al., *Nanosistemi, nanomateriali, nanotehnologyi*., **22**(2), 229-238. (2024).